We are IntechOpen, the world's leading publisher of Open Access books
Built by scientists, for scientists

5,900
Open access books available

145,000
International authors and editors

180M
Downloads

154
Countries delivered to

Our authors are among the

TOP 1%
most cited scientists

12.2%
Contributors from top 500 universities

BOOK CITATION INDEX
CLARIVATE ANALYTICS
INDEXED

WEB OF SCIENCE™

Selection of our books indexed in the Book Citation Index
in Web of Science™ Core Collection (BKCI)

Interested in publishing with us?
Contact book.department@intechopen.com

Numbers displayed above are based on latest data collected.
For more information visit www.intechopen.com

Optical Vortices in a Fiber:
Mode Division Multiplexing
and Multimode Self-Imaging

S.N. Khonina, N.L. Kazanskiy and V.A. Soifer
Image Processing Systems Institute of the Russian Academy of Sciences,
S.P. Korolyov Samara State Aerospace University,
Russia

1. Introduction

The optical vortices (Dennis et al., 2009; Desyatnikov et al., 2005; Soskin & Vasnetsov, 2001) or angular harmonics $\exp(im\varphi)$ describe a wavefront peculiarity, or helical dislocation, when in passing around the origin of coordinates the light field phase acquires a phase shift of $2\pi m$, where m is the optical vortex's order. The generation and propagation of the laser vortices in free space has been studied fairly well, meanwhile, the excitation of individual vortex modes and obtaining desired superpositions thereof in optical fibers present a greater challenge (Berdague & Facq, 1982; Bolshtyansky et al., 1999; Dubois et al., 1994; Karpeev & Khonina, 2007; Mikaelian, 1990; Soifer & Golub, 1994; Thornburg et al., 1994; Volyar & Fadeeva, 2002).

Note that the most interesting is the excitation and propagation of pure optical vortices that are not step- or graded-index fiber modes. However decomposition of the light fields in terms of angular harmonics has a number of advantages over other bases, including modal ones, when dealing with problems of laser beam generation and analysis and mode division multiplexing. As distinct from the classical LP-modes, the angular harmonics are scale-invariant when coupled into the fiber and selected at the fiber's output using diffractive optical elements (DOEs) (Dubois et al., 1994; Karpeev & Khonina, 2007; Soifer & Golub, 1994; Thornburg et al., 1994). This gives much freedom in choosing parameters of an optical scheme, allowing one to effectively counteract noises, as it will be demonstrated below.

A term "mode division multiplexing" (MDM) is used for multimodal optical fibers when describing methods for data transmission channel multiplexing, with each spatial fiber mode being treated as a separate channel that carries its own signal (Berdague & Facq, 1982; Soifer & Golub, 1994). The essence of mode division multiplexing is as follows: laser beams as a linear superposition of fiber modes can be used to generate signals that will effectively transmit data in a physical carrier - a multimodal fiber. The data transmitted can be contained both in the modal composition and in the energy portion associated with each laser mode.

The MDM concept has not yet been turned to practical use because a definite mode superposition with desired between-mode energy distribution is difficult to excite. Another reason is that there is energy redistribution between modes when transmitting data in real

fibers over long distances. However, for optical fibers 1-2 m long - for example, used in endoscopy - the modes do not mix at small bendings (when the curvature radius is much greater than fiber's core radius), acquiring only a radius-related phase delay.

A major problem with the MDM is exciting a definite modal superposition with a desired energy distribution between modes. Lower-order modes (e.g., LP11) can be excited by applying a periodic fiber deformation (squeezing or bending) and with a tilted grating written in a photosensitive fiber by two interfering laser beams. Higher-order modes LPm1 can be generated through the off-axis coupling of laser light into the fiber's end at a definite angle or by DOE in which the complex amplitude of mode distribution was encoded. Using diffractive optical elements any set of modes with designed weights can be effectively generated and selected (Soifer & Golub, 1994; Karpeev & Khonina, 2007).

We discuss linear superpositions of LP-modes of a stepped-index fiber in the first section. As an alternative to the superposition of classical LP-modes used to carry signal in a light fiber we propose a superposition of angular harmonics that can be derived as a special combination of LP-modes also featuring modal properties in an optical fiber.

Imposing the certain conditions on mode's compound it is possible to form laser beams with the definite self-reproduction (Kotlyar et al., 1998), while mode's weights and phase shift between modes provide approximation of desirable cross-section distribution of laser beam intensity on the certain distances (Almazov & Khonina, 2004).

The light field periodic self-reproduction in the gradient-index media was analytically studied using the ray tracing approach and wave theory in (Mikaelian, 1980). The self-reproduction was treated in the above studies as self-focusing, i.e. a periodic focusing of radiation. The analytical expressions for the refractive index of the medium where the phenomenon occurs have been derived.

In the second section we numerically simulate the behavior of multi-mode light fields in the circular parabolic graded-index fibers which propagate linearly polarized Laguerre-Gaussian (LG) modes in the weak guidance approximation. Analytical formulae describing the propagation of a linear composition of the LG modes in a fiber are rather simple, thus making it possible to simulate the propagation of a certain light field (image) along a definite fiber via decomposing it into the LG modes (Snyder & Love, 1987). Note that the accuracy of image representation is essential. The more modes are found in the linear combination, the more adequate is the image approximation. Also, with regard to the aforementioned application, it would be interesting to determine the self-reproduction periods of the chosen mode superposition.

Unfortunately, the use of an arbitrary number of modes satisfying definite criteria is impossible for the following two reasons: (1) a multi-mode fiber is able to transmit only a limited number of modes determined by its radius and the core's refractive index and (2) the more modes participate in the approximation, the greater is their general period, i.e. the image self-reproduction will occur more rarely. Besides, the image is disintegrated even under a minor change in the fiber length (of about 0.1.mm) as a result of temperature variations, mechanical deformation, etc. Thus, the "direct" image recognition from the intensity pattern becomes difficult if possible at all. However, the images can be fairly accurately recognized from the distribution pattern of the squared modules of the mode coefficients (Bolshtyansky & Zel'dovich, 1996), which are preserved at any distance in the ideal fiber.

The propagation of the electromagnetic wave in the medium can be modeled in several ways. The most common technique is to describe the propagation using Maxwell's

equations, from which vectorial wave equations defining the electric and magnetic field components can be deduced. If the relative change of the medium refractive index per wavelength is significantly smaller than unity, the Helmhotz equation can be written for each scalar component of the vector field (Agrawal, 2002).

For weakly nonuniform media, the approximation based on a periodic array of identical optical elements placed in a uniform medium is also valid. In particular, for the parabolic-index medium, this array comprises circular converging lenses. For the limiting case of an infinitely large number of lenses with an infinitesimally small separation we derive an integral operator to describe the propagation of light in a medium with parabolic refractive index in the scalar theory. This integral operator is analogous to the Fresnel transform that describes, with the same accuracy, the propagation of light in a uniform medium.

2. Vortical laser beams in a weakly guiding stepped-index fibers

Let us consider a circular stepped-index optical fiber, in which the core of radius a has the refractive index of n_1, and the cladding of radius b has the refractive index of n_2. For most popular commercial fibers, the core-cladding index contrast, $\Delta n = n_1 - n_2$, is less than 1%. For such fibers, termed weakly guiding, assuming $n_1 \cong n_2$, we can consider in place of hybrid modes of the propagating electromagnetic field their linearly polarized superpositions (Cherin, 1987; Gloge, 1971; Marcuse, 1972; Yeh, 1990).

Considering that for the LP-mode the transverse field is essentially linearly polarized, a complete set of modes takes place when only one electric and one magnetic component are predominant. In this case, it is possible, for example, to consider the electric vector **E** directed along the x-axis, and a perpendicular magnetic vector **H**, directed along the y-axis. Note, also, that the time-averaged power flux (Re[**E**×**H**]/2) appears to be proportional to the electric vector intensity (Gloge, 1971; Yeh, 1990). All above considered, we will consider the LP-modes in the scalar form:

$$\Psi_{pq}(r,\phi,z) = \exp\left(-i\beta_{pq}z\right)T_p(\phi)R_{pq}(r) = \exp\left(-i\beta_{pq}z\right)\begin{Bmatrix}\cos(p\phi)\\\sin(p\phi)\end{Bmatrix}\begin{cases}\dfrac{J_p(u_{pq}r/a)}{J_p(u_{pq})}, & 0 \le r \le a \\[3mm] \dfrac{K_p(w_{pq}r/a)}{K_p(w_{pq})}, & a \le r \le b\end{cases} \tag{1}$$

where the parameters

$$u = a\sqrt{\left(kn_1\right)^2 - \beta^2}, \tag{2}$$

$$w = a\sqrt{\beta^2 - \left(kn_2\right)^2}, \tag{3}$$

$$u^2 + w^2 = V^2 \equiv \left(\frac{2\pi}{\lambda}\right)^2 a^2\left(n_1^2 - n_2^2\right), \tag{4}$$

are derived from an equation for eigen-values:

$$\frac{uJ_{p-1}(u)}{J_p(u)} = -\frac{wK_{p-1}(w)}{K_p(w)}. \tag{5}$$

In Eq. (4), λ is the wavelength of laser light in air. In Eq. (1), the first-kind Bessel functions $J_m(x)$ describe the field in the fiber core, whereas the modified Bessel functions $K_m(x)$ are for the cladding.

We consider the propagation of a linear superposition of LP-modes in an ideal stepped-index optical fiber:

$$U_0(r,\phi) = \sum_{p,q \in \Omega} C_{pq}\Psi_{pq}(r,\phi) \tag{6}$$

where C_{pq} are the complex coefficients, $\Psi_{pq}(r,\varphi)$ are the modes of Eq. (1) at $z=0$, whose angular component is represented in a different way without loss of generality:

$$\Psi_{pq}(r,\phi,z) = \exp\left(-i\beta_{pq}z\right)\exp\left(ip\phi\right)\begin{cases} \dfrac{J_p(u_{pq}r/a)}{J_p(u_{pq})}, & 0 \le r \le a \\[3mm] \dfrac{K_p(w_{pq}r/a)}{K_p(w_{pq})}, & a \le r \le b \end{cases} \tag{7}$$

Although Eqs. (1) and (7) are connected via a simple relation, they describe modes with somewhat different properties. By way of illustration, the modes in Eq. (1) are real at $z=0$, but they do not have an orbital angular momentum. Thus, for each mode in Eq. (7), the linear density of z-projection of the orbital angular momentum is proportional to the first index p (Allen et al., 2003).

For the field in Eq. (6) with the modes of Eq. (7), the z-projection of the orbital momentum (Kotlyar et al., 2002):

$$J_{z0} = -\frac{\displaystyle\sum_{p,q \in \Omega} p\left|C_{pq}\right|^2}{\omega \displaystyle\sum_{p,q \in \Omega} \left|C_{pq}\right|^2} \tag{8}$$

The modes show a key property of invariance to the propagation operator in a given medium, implying that in propagation the mode structure remains unchanged, acquiring only a phase shift. In particular, the cross-section of the field in Eq. (7) will remain unchanged at any distance, being equal to its value at $z=0$:

$$\left|\Psi_{pq}(r,\phi,z)\right|^2 = \left|R_{pq}(r)\exp(ip\phi)\exp(-i\beta_{pq}z)\right|^2 = R_{pq}^2(r) = \left|\Psi_{pq}(r,\phi)\right|^2. \tag{9}$$

Because the expression in Eq. (9) is z-independent in a perfect fiber, it can be used as an additional parameter to characterize individual modes in Eq. (7) or modal groups with an identical first index.

Figure 1 shows cross-section distributions for some modes of Eq. (7) for a stepped-index fiber with cut-off number $V=8.4398$. These modal characteristics remain unchanged upon propagation in a perfect fiber, with only phase changes taking place. For comparison, shown in Figs. 1d and 1e are phases at z=0 and z=100 μm, respectively.

The numerical simulation parameters are as follows: core radius is a=5 μm, cladding radius is b=62.5 μm, the respective refractive indices of the core and cladding are n_1=1.45

and n_2=1.44. Optical fibers with the above-specified parameters are normally used in a unimodal regime for wavelengths λ=1.31 μm and λ=1.55 μm. However, for the wavelength of λ=0.633 μm of a He-Ne laser a few-mode regime occurs (Khonina et al., 2003), meaning that several modes are propagated. For used parameters there are 11 propagating modes with |p|≤5.
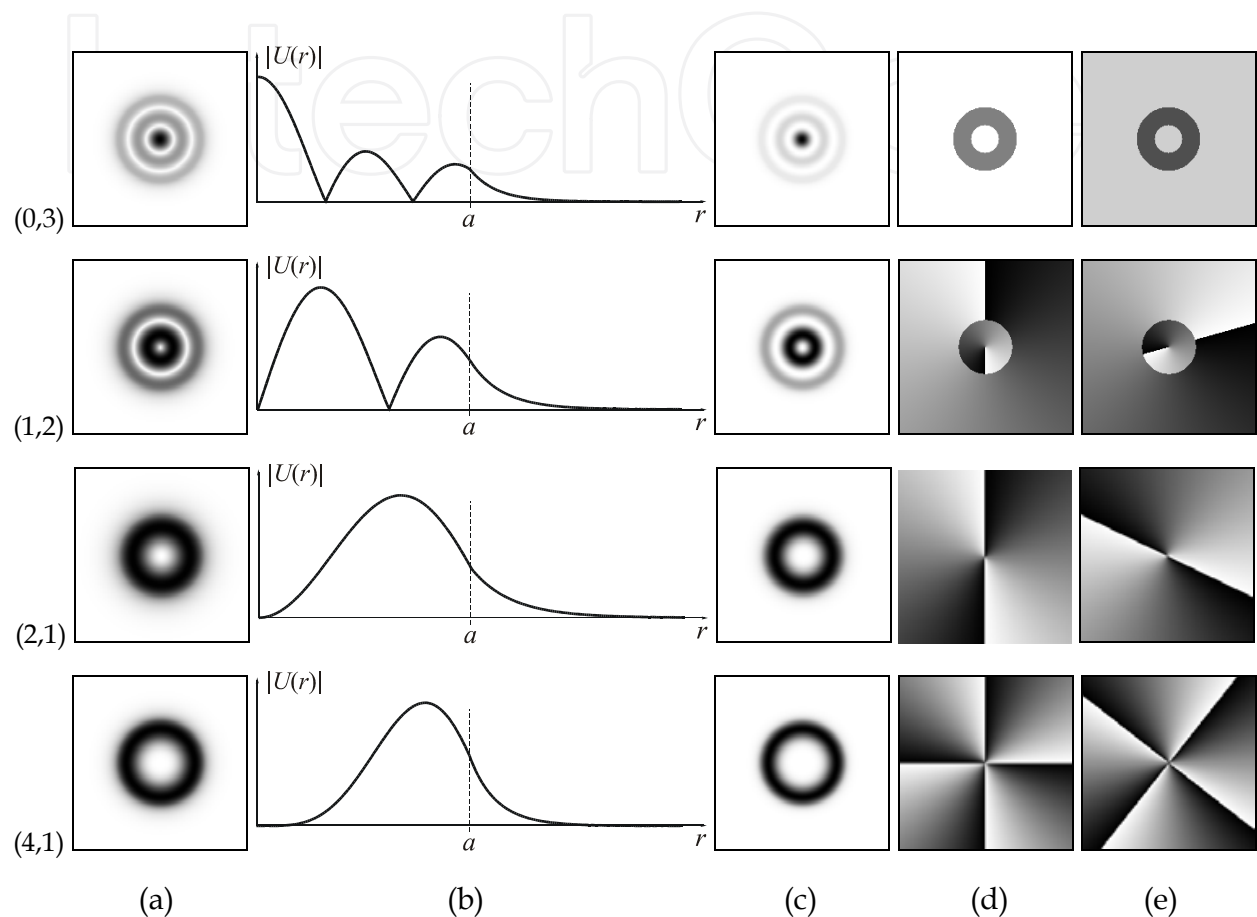

Fig. 1. The (p,q) modes: (0,3), (1,2), (2,1), (4,1): (a) transverse amplitude distribution (negative), (b) radial amplitude cross-section, and (c) transverse intensity distribution (negative) in the plane z=0; transverse phase distribution (white: zero phase, black: 2π) in the planes (d) z=0 and (e) z=100 μm.

2.1 Multimode laser beam self-imaging in a weakly guiding stepped-index fibers

In the general case, the field in Eq. (6) does not show invariance regarding an individual mode in Eq. (9). However, by fitting a modal composition in Eq. (6) it is possible to find a modal superposition showing some self-reproduction properties.

In a perfect fiber at distance z, the superposition in Eq. (6) has the complex distribution

$$U(r,\phi,z) = \sum_{p,q\in\Omega} C_{pq}\Psi_{pq}(r,\phi,z), \qquad (10)$$

where $\Psi_{pq}(r,\phi,z) = \Psi_{pq}(r,\phi)\cdot\exp(-i\beta_{pq}z)$, β_{pq} are the propagation constants.

For any pair of modes, the intensity at distance z

$$\left| C_{p_i q_i} \Psi_{p_i q_i}(r,\phi,z) + C_{p_j q_j} \Psi_{p_j q_j}(r,\phi,z) \right|^2 = \left| C_{p_i q_i} \right|^2 R^2_{|p_i|q_i}(r) + \left| C_{p_j q_j} \right|^2 R^2_{|p_j|q_j} +$$
$$+ 2 \left| C_{p_i q_i} \right| \left| C_{p_j q_j} \right| R_{|p_i|q_i}(r) R_{|p_j|q_j}(r) \cos \left[(\arg C_{p_i q_i} - \arg C_{p_j q_j}) + (p_i - p_j)\phi + (\beta_{|p_i|q_i} - \beta_{|p_j|q_j})z \right] \tag{11}$$

is other than the intensity at $z=0$:

$$\left| C_{p_i q_i} \Psi_{p_i q_i}(r,\phi) + C_{p_j q_j} \Psi_{p_j q_j}(r,\phi) \right|^2 = \left| C_{p_i q_i} \right|^2 R^2_{|p_i|q_i}(r) + \left| C_{p_j q_j} \right|^2 R^2_{|p_j|q_j} +$$
$$+ 2 \left| C_{p_i q_i} \right| \left| C_{p_j q_j} \right| R_{|p_i|q_i}(r) R_{|p_j|q_j}(r) \cos \left[(\arg C_{p_i q_i} - \arg C_{p_j q_j}) + (p_i - p_j)\phi \right] \tag{12}$$

because the former has a cosine term.

By imposing definite conditions on all pairs of constituent modes in the superposition in Eq. (6), it is possible to obtain fields featuring special properties of intensity distribution self-reproduction.

Invariance in the entire region of propagation

In propagation, a change in the transverse field distribution is due to intermode dispersion caused by a difference between mode propagation constants β_{pq}. For the function of the form (7) only modes with identical indices ($|p|,q$) will have the same propagation velocities. Thus, at any interval (in a perfect fiber) the invariance is shown only by a mode pair superposition given by

$$C_{|p|q} \Psi_{|p|q}(r,\phi) + C_{-|p|q} \Psi_{-|p|q}(r,\phi) . \tag{13}$$

In this case, in Eq. (11) we have

$$\cos \left[(\arg C_{|p|q} - \arg C_{-|p|q}) + (|p| + |p|)\phi + (\beta_{|p|q} - \beta_{-|p|q})z \right] = \cos \left[(\arg C_{|p|q} - \arg C_{-|p|q}) + 2|p|\phi \right]$$

and the cross-section intensity ceases to depend on z, remaining unchanged. The form of the intensity distribution is entirely determined by the coefficients C_{pq} (see Fig. 2).

In a particular case, when $\left| C_{|p|q} \right| = \pm \left| C_{-|p|q} \right|$ we get classical LP-modes in the form of Eq. (1) (first row in Fig. 2). It is noteworthy that the complex coefficient arguments have no effect on the value of the orbital angular momentum for the superposition of Eq. (6). Thus, with the coefficient amplitudes remaining unchanged, we obtain a rotated classical LP-mode whose orbital angular momentum is also zero (second row in Fig. 2).

Changes in the coefficient amplitude cause both the cross-section structure and the orbital angular momentum to be changed. For the third and bottom rows in Fig. 2, the respective values of the orbital angular momentum in Eq. (8) are different and equal to 0.6 and 0.923.

Invariance on the interval [0,z].

Besides, superpositions that approximately (to some accuracy) preserve the cross-section intensity distribution may be of interest. In this case, for all constituent mode pairs the following condition should be met:

$$\left| \cos \left[(p_i - p_j)\phi + (\beta_{p_i q_i} - \beta_{p_j q_j})z \right] - \cos \left[(p_i - p_j)\phi \right] \right| < \varepsilon , \tag{14}$$

where ε is small and defines the "recession" of different modes on the z-axis. Such between-mode "delay" can be defined as a small phase shift ϕ_ε:

$$\left| \beta_{p_i q_i} - \beta_{p_j q_j} \right| z \le \varphi_\varepsilon .$$ (15)
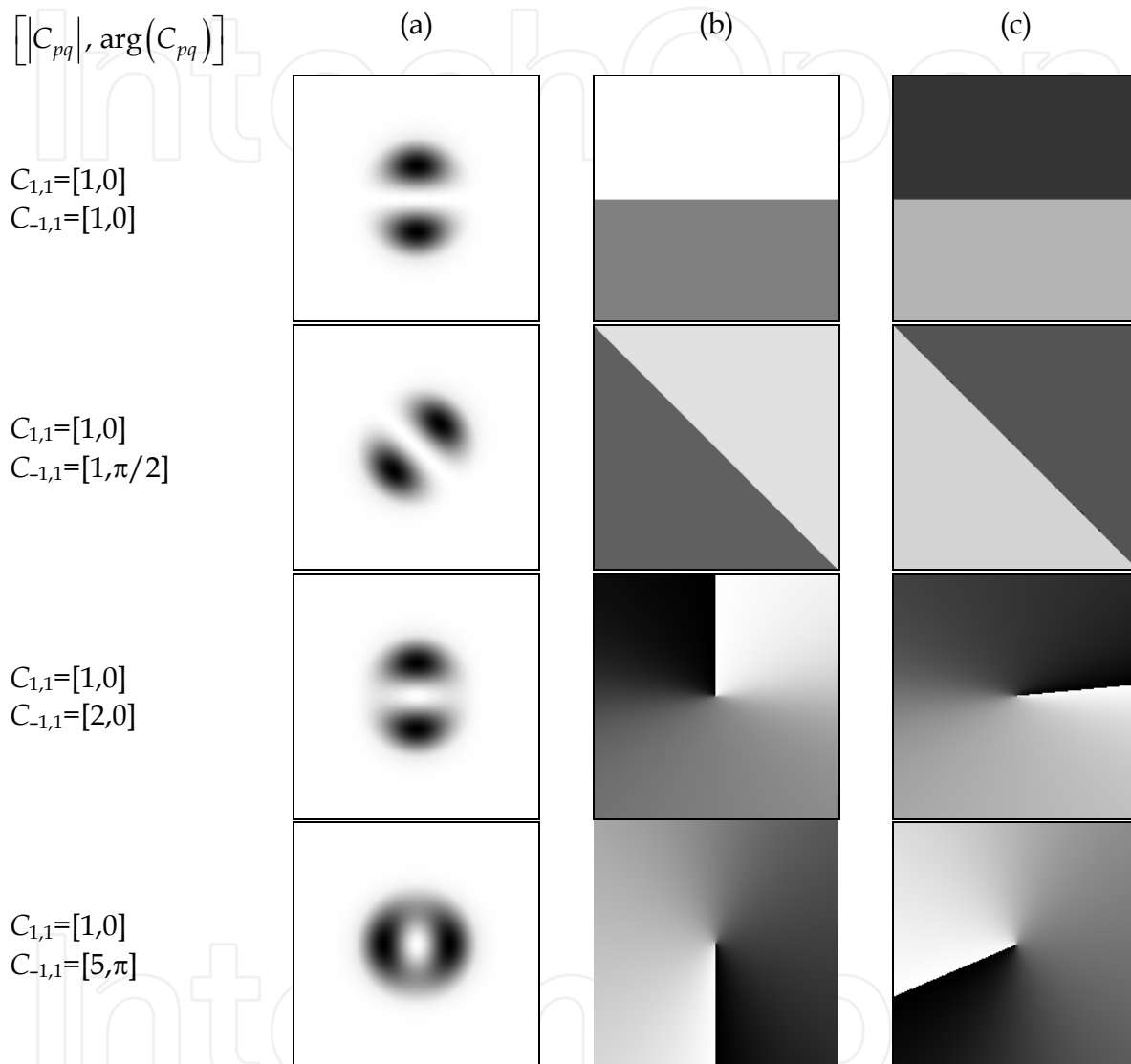

Fig. 2. Superposition of the (p,q) modes: $(1,1)+(-1,1)$ with different complex coefficients: transverse distribution of (a) intensity, and (b) phase in the plane $z=0$, and (c) phase distribution at distance $z=200$ m.

Formalizing the condition of the interval-specific invariance to a desired accuracy makes possible an automated procedure for selecting admissible superpositions from the entire set of fiber modes. The algorithm can be realized as an exhaustive search of modes with selection of superpositions satisfying the condition formulated.

For instance, putting on the 10 μm interval the admissible phase shift equal to $\phi_\varepsilon = \pi/18$, the algorithm allowed us to select 59 superpositions (containing 2-5 modes, regarding the index p sign) from the set of 11 propagating modes for used parameters.

Figure 3 shows the transverse distributions of amplitude, intensity, and phase at different distances for a single superposition, namely, (p,q): $(1,2)+(–1,2)+(3,1)+(–3,1)$, with the C_{pq} coefficients chosen to be the same.

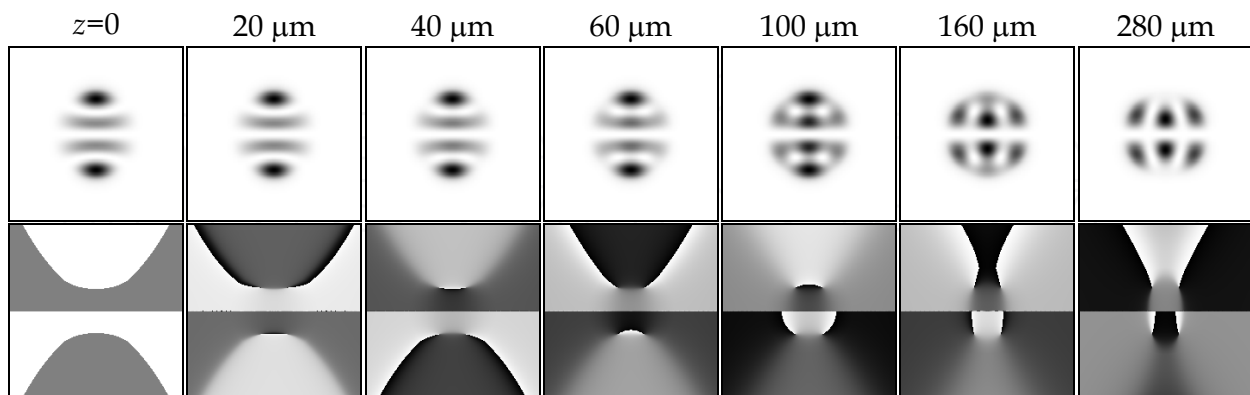| z=0	20 μm	40 μm	60 μm	100 μm	160 μm	280 μm

Fig. 3. Propagation of the superposition (p,q): $(1,2)+(–1,2)+(3,1)+(–3,1)$: transverse distributions of intensity (top row), and phase (bottom row) at different distances z.

As seen from Fig. 3, intensity of the multimode beam remains practically constant up to distance 40 μm. Unfortunately, since intermode dispersion in a stepped-index fiber being very high, putting the phase shift $\phi_\varepsilon \leq \pi/18$ makes possible only 17 superpositions on the 20 μm interval and 8 superpositions on the interval 40 μm. Note that there are just 8 superpositions of Eq. (10) which are admissible on any interval.

The number of superpositions that preserve their form on any interval can be essentially extended if considering a rotation-accurate invariance or "rotating" fields.

All-region, rotation-accurate propagation invariance

Assuming rotation-accurate invariance, mode pairs in the superposition must obey the following condition:

$$\cos\left[(p_i - p_j)\phi + (\beta_{|p_i|q_i} - \beta_{|p_j|q_j})z\right] = \cos\left[(p_i - p_j)(\phi + \phi_0)\right], \tag{16}$$

where ϕ_0 is some angle.

From Eq. (16), the rotation condition for any pair in the superposition is

$$\frac{\beta_{|p_i|q_i} - \beta_{|p_j|q_j}}{p_i - p_j} z = \phi_0, \tag{17}$$

The exact condition in Eq. (17) complies with any two-mode superpositions, given $|p_i| \neq |p_j|$, since at $|p_i| = |p_j|$ there will occur the rotation by angle ϕ_0=0, i.e. the total invariance dealt with in the previous section. Thus, exciting various mode pairs enables obtaining fields that preserve their structure (except for rotation) at any interval. There may be 154 such superpositions, which exceeds 8 purely invariant syperpositions. By way of illustration, Fig. 4 shows the propagation at distance 150 m of invariant, rotating mode pairs.
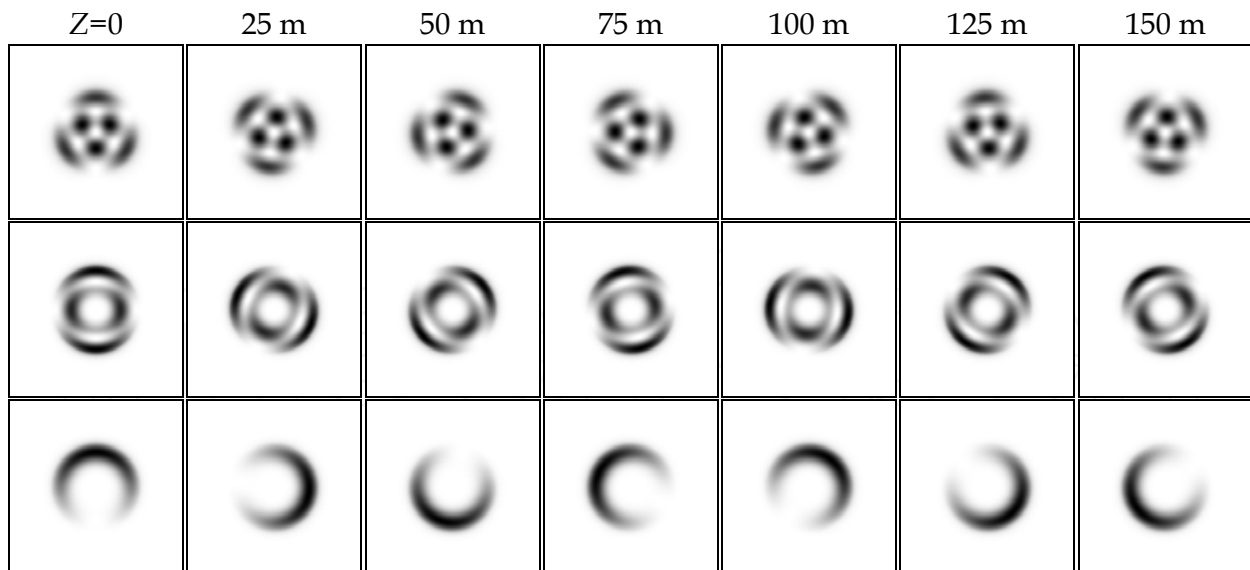
Z=0	25 m	50 m	75 m	100 m	125 m	150 m

Fig. 4. Propagation of rotating modal pairs, (p,q): (1,2)+(–2,1) – top row, (3,2)+(5,1) – middle row, (4,1)+(5,1) – bottom row; the intensity distribution is shown at different distances z.

From Fig. 4, the superpositions are seen to have symmetry of order

$$s = \left| p_1 - p_2 \right|. \tag{18}$$

Note that due to symmetry, the transverse intensity distribution is self-reproduced s times at a distance of one full revolution.

For such a pair, the rotation rate is given by

$$\vartheta = \frac{\beta_{|p_1||q_1} - \beta_{|p_2||q_2}}{p_1 - p_2}, \tag{19}$$

with the rotation direction corresponding to the sign of Eq. (18).

It is noteworthy that the rotation rate of interference pattern for the constituent modes in Eq. (19) is not related to the orbital angular momentum, depending on the propagation constants rather than the mode coefficients. In particular, for the mode pairs in Fig. 4, considering equal coefficients, Eqs. (9) and (24) take the values: for (1,2)+(–2,1), $\omega J_{z0}=0.5$, $\vartheta=0.54$; for (3,2)+(5,1), $\omega J_{z0}=-4$, $\vartheta=-0.35$; and for (4,1)+(5,1), $\omega J_{z0}=-4.5$, $\vartheta=1.02$.

Note that the transverse energy distribution of a beam composed of two modes can be varied by varying the mode coefficients. The intensity distribution itself will be preserved in propagation in a perfect fiber.

Rotation-accurate invariance on the [0,z] interval

Rotating superpositions containing more than two modes become possible by assuming a small error in the self-reproduction of the transverse intensity distribution. In this case, the following condition should be met for any two modal pairs in the superposition, (p_i,q_i)+(p_j,q_j) and (p_k,q_k)+(p_l,q_l):

$$\max \Delta_{ij}^{kl} - \min \Delta_{ij}^{kl} \leq \phi_\varepsilon, \tag{20}$$

where $\Delta_{ij}^{kl} = \phi_{ij} - \phi_{kl}$, $\phi_{ij} = \left| \dfrac{\beta_{p_i q_i} - \beta_{p_j q_j}}{p_i - p_j} \right| z$, φ_ε is the admissible rotation mismatch angle on the entire interval $[0,z]$.

Figure 5 shows the propagation of a superposition of three modes (p,q): $(2,2)+(-4,1)+(5,1)$ with identical coefficients at distance 1500 μm. This superposition obeys the condition in Eq. (25) with admissible mismatch angle of $\varphi_\varepsilon \leq \pi/36$ on the interval up to 150 μm. The $(-2,2)+(4,1)+(-5,1)$ superposition, with symmetric index signs, shows a similar property. No other more-than-two modal combinations were found.

| $Z=0$ | 75 μm | 150 μm | 225 μm | 300 μm | 750 μm | 1500 μm |

Fig. 5. Propagation of a superposition of (p,q): $(2,2)+(-4,1)+(5,1)$: transverse distributions of intensity at different distances z.

It is seen from the above that the more-than-two-mode superpositions preserve their structure at a short interval of about one hundred microns, followed by the structure's disintegration. After a while (period), however, the beam cross-section is self-reproduced.

Periodic self-reproduction

For a two-mode superposition there is always a self-reproduction period z_0 defined as

$$\cos\left[(p_1 - p_2)\phi + (\beta_{p_1 q_1} - \beta_{p_2 q_2})z_0 \right] = \cos\left[(p_1 - p_2)\phi \right] \Rightarrow \left| \beta_{p_i q_i} - \beta_{p_j q_j} \right| z_0 = 2\pi m, \qquad (21)$$

where m is integer.

However, once the distance z_L is set, it would be of greater interest to identify possible modal superpositions that will be self-reproduced at this distance to a certain admissible accuracy. Such superpositions can be formed as mode pairs satisfying the condition:

$$\left| \left[(\beta_{p_i q_i} - \beta_{p_j q_j})z_L \right]_\pi \right| \leq \varphi_\varepsilon , \qquad (22)$$

where ϕ_ε is the admissible, reduced phase shift and $[\ldots]_\pi$ denotes reduction to the interval $[-\pi,\pi]$.

For example, putting $z_L=1089.4$ um (which is close to the self-reproduction period for two modes, $(0,3)+(5,1)$), specifying the admissible reduced phase shift equal to $\phi_\varepsilon \leq \pi/12$ allows a set of 41 admissible superpositions, each containing 2-5 modes, to exist. In particular, Fig. 6 shows how a five-mode superposition, (p,q): $(0,3)+(3,2)+(-3,2)+(5,1)+(-5,1)$, propagates at the interval from $z=0$ to z_L. In the z_L-plane the superposition is self-reproduced with an error of $\delta=0.48\%$ for intensity. Note that the complex field correlation at $z=0$ and z_L is close to unity: $\eta=0.989$.

It is noteworthy that at a half-period distance, $z_L/2 = 544.7$ μm, the transverse intensity distribution equals the original one rotated by 180 degrees (see fig. 6). Thus, it is possible to

increase the number of points where a field is self-reproduced if considering the rotation-accurate self-reproduction.
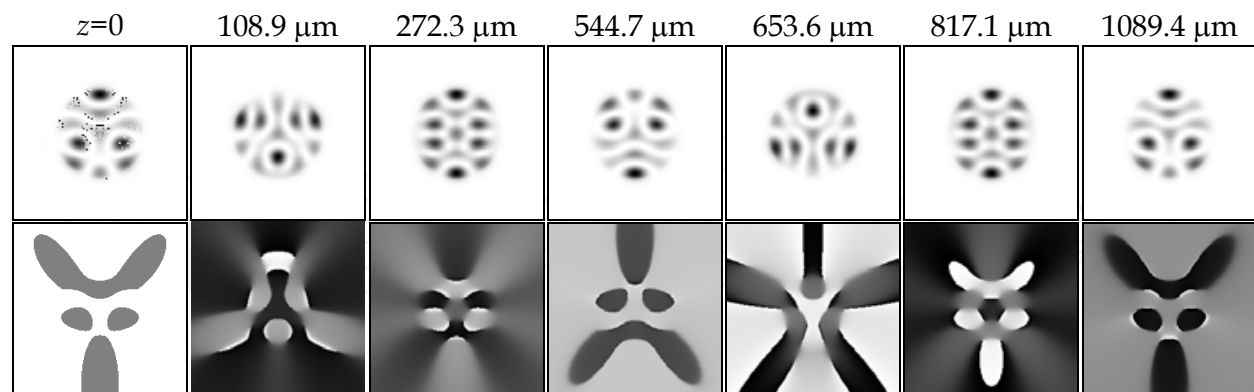
$z=0$	108.9 μm	272.3 μm	544.7 μm	653.6 μm	817.1 μm	1089.4 μm

Fig. 6. In propagation, the superposition of (p,q) modes: $(0,3)+(3,2)+(-3,2)+(5,1)+(-5,1)$ is nearly self-reproduced at distance $z_L=1089$ μm (intensity and phase distributions are depicted at various distances z).

Periodic rotation-accurate self-reproduction

Similar to the previous section, putting the distance z_L (e.g. fiber's length), we consider mode superpositions self-reproduced at this distance (period) up to a rotation-angle, with an admissible mismatch (otherwise, the set will only contain two-mode superpositions). In this case, the mode pairs in superposition should obey the condition:

$$\max \Delta_{ij}^{kl} - \min \Delta_{ij}^{kl} \le \phi_\varepsilon , \qquad (23)$$

where $\Delta_{ij}^{kl} = \left| \left[\phi_{ij} - \phi_{kl} \right]_\pi \right|, \phi_{ij} = \dfrac{(\beta_{p_i q_i} - \beta_{p_j q_j}) z_L}{p_i - p_j}$, φ_ε is the admissible mismatch angle in the z_L-plane.

Putting $z_L = 1$ m and the admissible mismatch angle equal to $\varphi_\varepsilon \le \pi/9$, it is possible to obtain a set of 173 allowed superposition, each containing from 2 to 3 modes. Figure 7 shows the propagation of a three-mode superposition of (p,q): $(2,1)+(3,1)+(4,1)$ on the interval from $z=0$ to z_L (at point $z_L = 1$ m, the mismatch angle being $\varphi_\varepsilon \le \pi/30$).

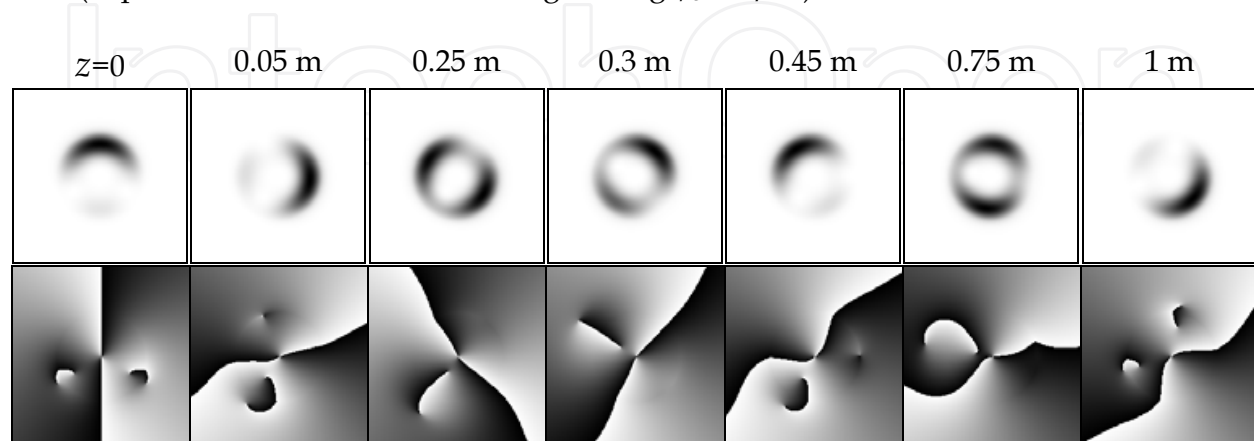| $z=0$	0.05 m	0.25 m	0.3 m	0.45 m	0.75 m	1 m

Fig. 7. In propagation, the superposition of (p,q) modes: $(2,1)+(3,1)+(4,1)$, is nearly self-reproduced at distance $z_L=1$ m (intensity and phase distributions are depicted at various distances z).

From Fig. 7, the superposition's intensity is also seen to be self-reproduced (to some accuracy) in other planes. However, this work was not aimed at identifying all points of self-reproduction for a definite superposition. The problem addressed was as follows: based on given physical characteristics of a stepped-index optical fiber (thickness, length, and parameters of material) it was required to identify the entire possible set of propagating modes and modal superpositions that show various self-reproduction properties to a designed accuracy.

2.2 Experimental excitation and detection of angular harmonics in a stepped-index optical fiber

When angular harmonics (optical vortices) are coupled into a fiber or selected at output using DOEs they show the scale invariance that provides much freedom in choosing optical scheme parameters. As shown below, this provides effective means for preventing system noise.

We describe natural experiments on selective excitation of both separate angular harmonics and their superposition. We used a DOE that was able to form beams with phase singularity $\exp(im\varphi)$ of order $m=-1$ and $m=-2$ and a superposition $\exp(im_1\varphi)+\exp(im_2\varphi)$, $m_1=-1$, $m_2=2$ (see Fig. 8). The multi-level DOEs were fabricated using e-beam lithography at the University of Joensuu (Finland). The DOEs parameters are: 32 quantization levels, diameter is 2.5 mm, and discretization step is 5 μm. Spiral DOEs were fabricated for wavelength λ=633 nm.

Selection was performed using multi-order DOEs (Khonina et al., 2003) matched to angular harmonics, which were also fabricated at Joensuu University. Shown in Fig. 9 is the 8-order binary DOE to detect spiral singularities with different numbers.
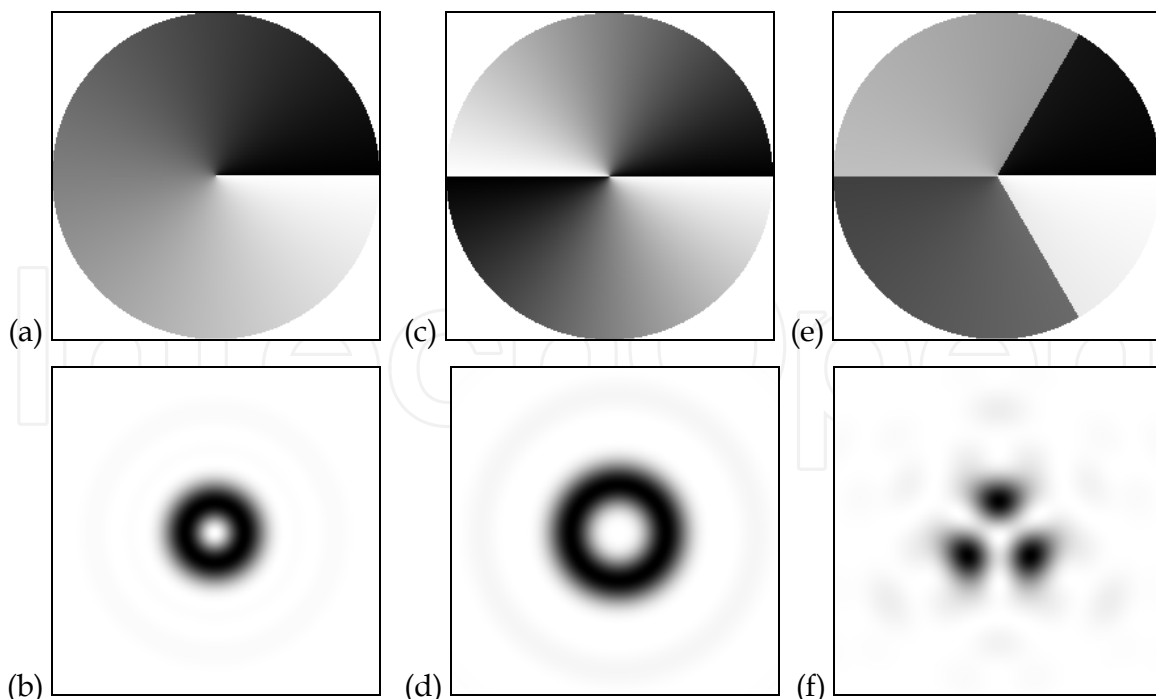
Fig. 8. Generation of light fields with phase singularity $\exp(in\varphi)$: DOE phase for (a) m=−1, (c) m=−2 and (e) a superposition of m_1=−1 and m_2=2, and (b), (d), (f) corresponding far-field intensity distributions.

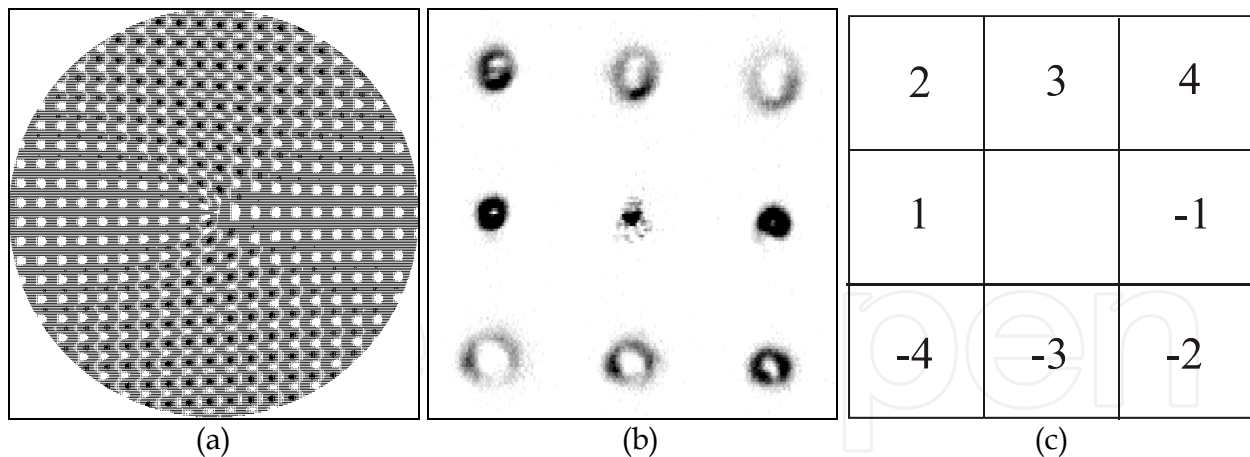|		
2	3	4
1		-1
-4	-3	-2

| (a) | (b) | (c) |

Fig. 9. Binary DOE matched to 8 different number angular harmonics: (a) phase, (b) corresponding patterns for the diffraction orders for plane wave and (c) the accordance scheme of angular harmonics' numbers and diffraction orders.

Diffraction order patterns are also put in correspondence with the numbers of the angular harmonics. The DOE parameters are: diameter is 10 mm, discretization step is 5 μm, and microrelief height for wavelength λ=633 nm.

First, following the procedure described in (Karpeev et al., 2005), the system was adjusted for coupling the principal mode. At this stage, the mode-generating DOE's substrate, being already put into the beam, is displaced to prevent the phase microrelief region from getting into the beam path. At the output, the Gaussian beam of the principal mode is collimated and then passed through a DOE matched to the angular harmonics and a Fourier stage. The scale at the Fourier stage output plane is related to both the output beam's diameter and the Fourier stage focal length. For angular harmonics, these parameters can be independently changed, as distinct from the classical modes where the beam size is rigidly connected with the DOE parameters. Besides, increasing focal length and correspondingly increasing scale help reduce noise. This is due to the high-frequency nature of noises resulting from high-frequency discretization of the phase DOEs, with noise level becoming lower closer to the optical axis. Thus, with the optical system's overall size allowing a decrease, for the noise impact to be reduced, lower carrier frequencies need to be chosen (on the assumption that there is no order overlapping).

The experiments were conducted with three beam-generation DOEs, which, accordingly, generated the first- and second-order angular harmonics as well as their superposition are coupled into a fiber. Figure 10 shows intensity distributions in the output plane when the corresponding beam is excited in a fiber.

When a first-order optical vortex is excited the intensity peak appears at the center of the corresponding order with the near-noise intensity (no more than 10% of peak intensity) found at the other orders (fig. 10a). Next, a second-order optical vortex was excited (fig. 10b). It was found that depending on the position of the beam-generation DOE in the illuminating beam, the intensity peak can emerge in diffraction orders corresponding to the second-order harmonics of both signs. It is possible to excite both any separate mode and their combination featuring about the same intensity. Note, however, that in this case the excitation selectivity is lower, compared with the first-order harmonic.

A third experiment was on excitation of a superposition of the opposite-sign, first- and second-order angular harmonics (fig. 10c). The emergence of the first- and second-order
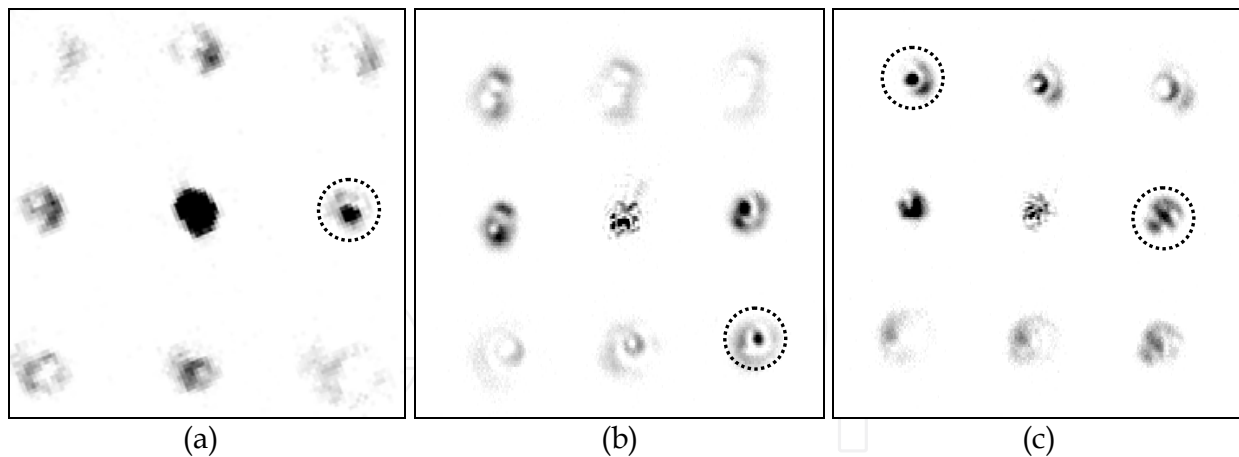
Fig. 10. Output intensity distributions for different angular harmonic coupled into a fiber:
(a) m=–1, (b) m=–2 and (c) a superposition of m_1=–1 and m_2=2.

singularity, with central intensity maximum seen at the corresponding orders and near-noise intensity at the other orders (no more than 15% of maximum). It should be noted that the maximum corresponding to the second-order angular harmonic is 10% weaker than the maximum of the first-order harmonic. It may be due to inadequate resolution, because space resolution requirements for different-order angular harmonics are different.

3. Multimode self-imaging in a weakly guiding parabolic fiber

In a gradient parabolic fiber, the refractive index is given by

$$n^2(r) = n_0^2 \left(1 - 2\Delta \frac{r^2}{r_0^2} \right) = n_0^2 \left(1 - \alpha^2 r^2 \right),$$
(24)

where r is the radius of the cylindrical coordinate system; n_0 is the refractive index on the fiber's optical axis; r_0 is a characteristic fiber radius; Δ is the dispersion parameter of the medium refractive index; and $\alpha = \sqrt{2\Delta}/r_0$ is a constant that defines the curvature of the refractive index profile.

It has been known (Snyder & Love, 1987; Soifer & Golub, 1994) that the solution of the Helmholtz equation in the cylindrical coordinates is given by the superposition of the Laguerre-Gaussian (GL) modes

$$\Psi_{nm}(r,\varphi,z) = \frac{1}{\sigma_0} \sqrt{\frac{n!}{\pi(n+|m|)!}} \cdot \left(\frac{r}{\sigma_0} \right)^{|m|} L_n^{|m|} \left(\frac{r^2}{\sigma_0^2} \right) \exp\left(-\frac{r^2}{2\sigma_0^2} \right) \exp(im\varphi) \exp(\pm i\beta_{nm}z),$$
(25)

where $L_n^m(\xi) = \frac{1}{n!} e^{\xi} \xi^{-m} \frac{d^n}{d\xi^n} \left\{ e^{-\xi} \xi^{n+m} \right\}$ are the Laguerre polynomials, $\sigma_0 = \left(\lambda r_0 / \pi n_0 \right)^{1/2} \left(2\Delta \right)^{-1/4}$ is the effective radius of the LG modes, $\beta_{nm} = \left[k^2 n_0^2 - 4\left(2n + |m| + 1 \right) / \sigma_0^2 \right]^{1/2}$ is a parameter proportional to the mode phase speed, n is a non-negative integer number, m is integer.

Propagation of an image in an ideal weakly guiding graded-index fiber can be described through a superposition of LG modes (Almazov & Khonina, 2004; Kotlyar et al., 1998). The approximation of an arbitrary image by the LG mode superposition is given by

$$F(r,\varphi) = \sum_{n,m\in\Omega} C_{nm}\Psi_{nm}(r,\varphi), \tag{26}$$

where coefficients C_{nm} can be derived from

$$C_{nm} = \int\limits_{0}^{\infty}\int\limits_{0}^{2\pi} F(r,\varphi)\Psi_{nm}^{*}(r,\varphi)\,r\,\mathrm{d}r\,\mathrm{d}\varphi \cdot \tag{27}$$

Then the beam (26) propagated distance z will have the following appearance

$$F(r,\varphi,z) = \sum_{n,m\in\Omega} C_{nm}\Psi_{nm}(r,\varphi,z) \cdot \tag{28}$$

The cut-off condition is taken from

$$kn_0 \le \beta_{nm} \le kn_0\sqrt{1-2\Delta} \cdot \tag{29}$$

Modelling the propagation of different test images (a cross, a triangle, a line-segment) through a fiber produces similar results: the image is disintegrated at a distance of about 0.1 mm, whereas the coefficient distribution is preserved at any distance to a 0.2% accuracy, which is close to the computation error (see Figs. 11-13). Hence, we can infer that the image recognition from the distribution of squared modules of the expansion coefficients C_{nm} has advantages over intensity-based recognition, on the understanding that the fiber has no considerable nonhomogeneities and bending resulting in changed coefficients and energy redistribution between the modes.
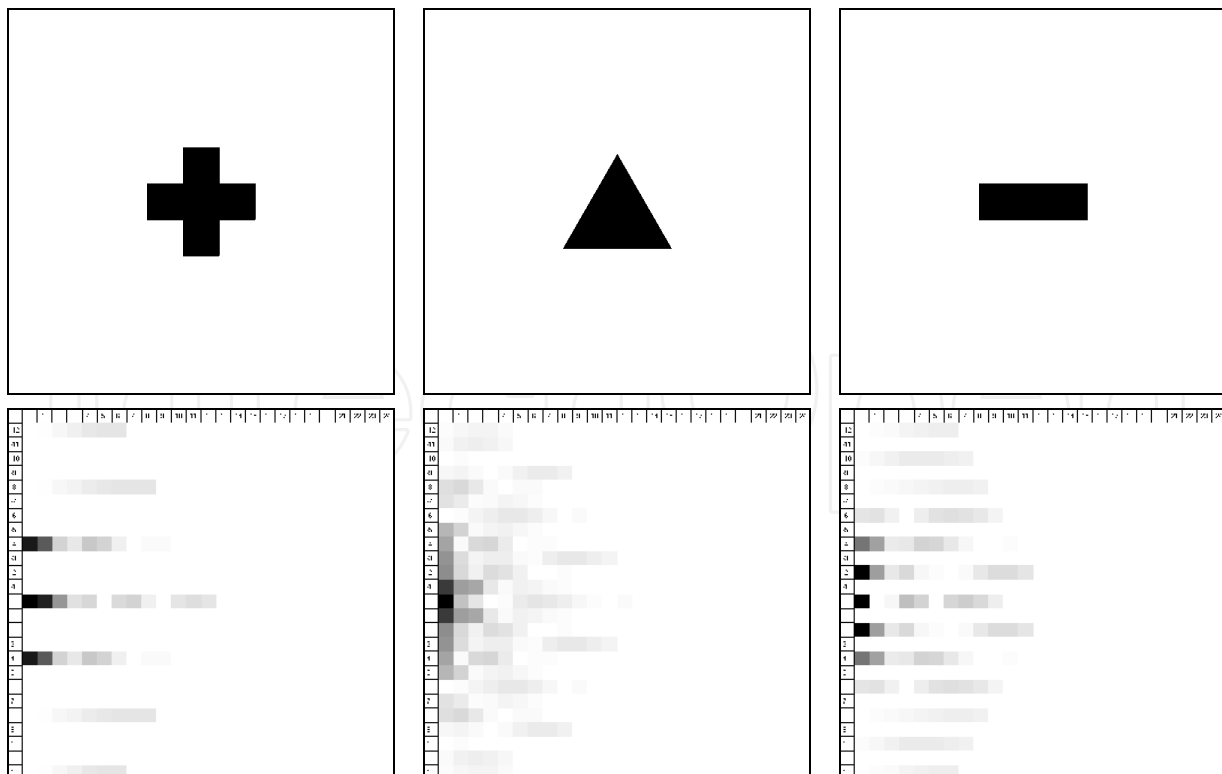

Fig. 11. Distribution of the squared modules of the coefficients of image expansion into the LG modes.

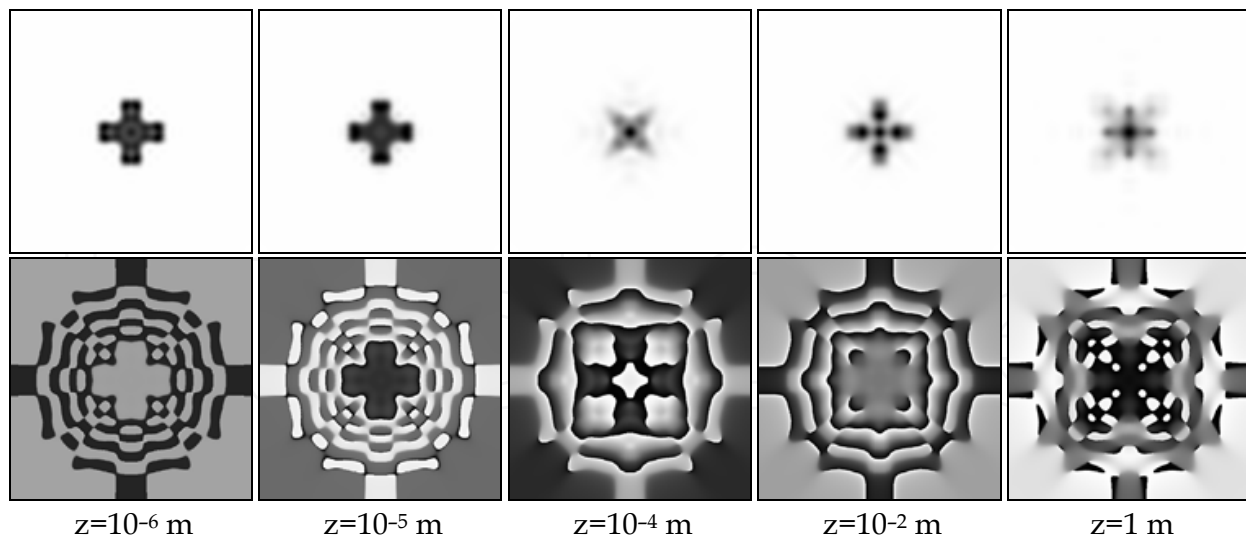| z=10⁻⁶ m | z=10⁻⁵ m | z=10⁻⁴ m | z=10⁻² m | z=1 m |

Fig. 12. Intensity and phase distribution for the cross image decomposition at different distances.
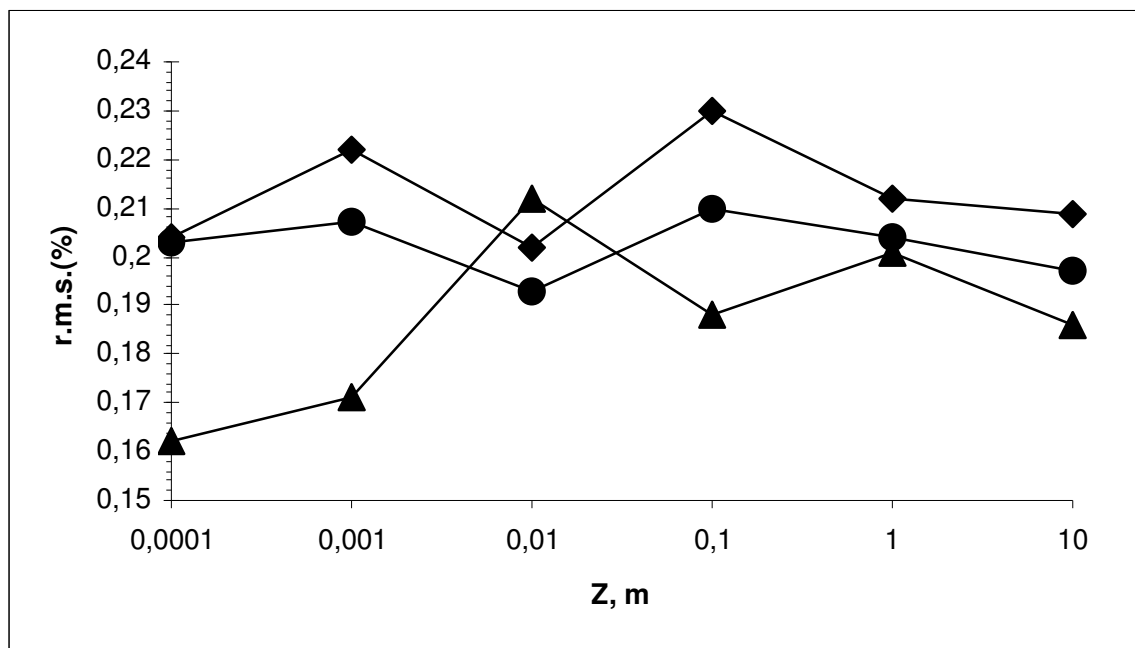

Fig. 13. The r.m.s. of the squared modules of amplitude coefficients C_{nm} (%) vs distance (♦ - cross, • - triangle and ▲ - horizontal line-segment).

3.1 Self-imaging in a weakly guiding parabolic fiber

From expression (25) it is possible to define the period of self-reproduction z_{nm} for each single mode in the superposition (28). The image will be periodically reproduced at a distance Z, such that Z/z_{nm} is an integer for any n, m of the constituent modes found in the composite image. Since the z_{nm} are irrational in the general case, there is no a general period even for a two-mode composition. However, we are able to obtain local self-reproduction periods where the image is reproduced to a sufficient accuracy. After the image has

propagated through several such distances the phase mismatch error will increase until it reaches a margin of visible image disintegration. However, having passed some distance the image will again enter a certain local stability zone with approximate self-reproduction points found at close intervals. It stands to reason that the greater number of modes are included into the image approximation, the greater is the self-reproduction period. For an ideal image composed of infinite number of modes the period is equal to infinity, i.e. there are no self-reproduction points. Thus, to be able to visually recognize the images we must impose an additional strict limitation on the approximation quality. Figures 14 and 15 show the patterns of the intensity and phase for the cross image at different distances in a circular graded-index fiber with parabolic refractive index distribution and the following parameters: r_0=25 μm; n_0=1.5; Δ=0.01; λ=0.63 μm.

It is seen from Figs. 14 and 15 that the cross image within the fiber has a local period of about 1.105 mm (the first group of self-reproduction points) and a large period of about 2.9 m (the second group of self-reproduction points). From Fig. 15 it is seen that after 2.9 m the reproduced image very closely matches the initial image (Fig. 14, z=0). Obviously, there are larger self-reproduction periods at which the superposition is reproduced to a greater accuracy.
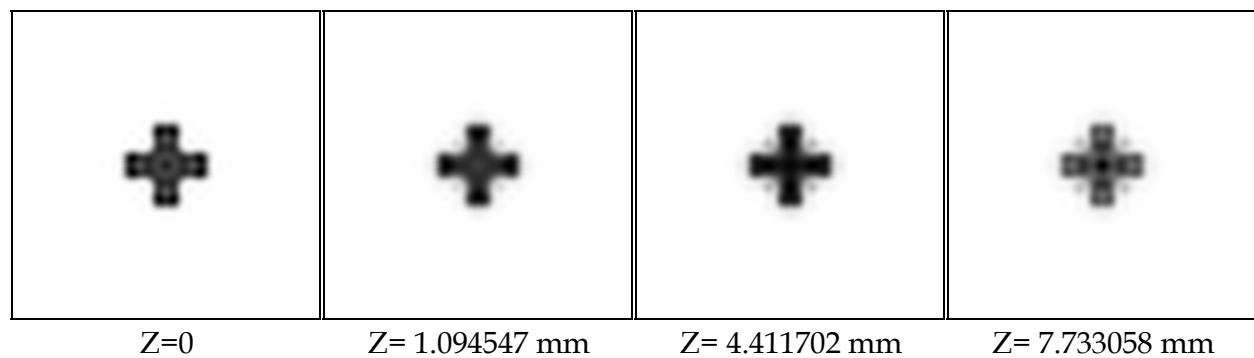
| Z=0 | Z= 1.094547 mm | Z= 4.411702 mm | Z= 7.733058 mm |

Fig. 14. Image self-reproduction – the "cross" image decomposition at different distances **z** from the first group of image self-reproduction points.
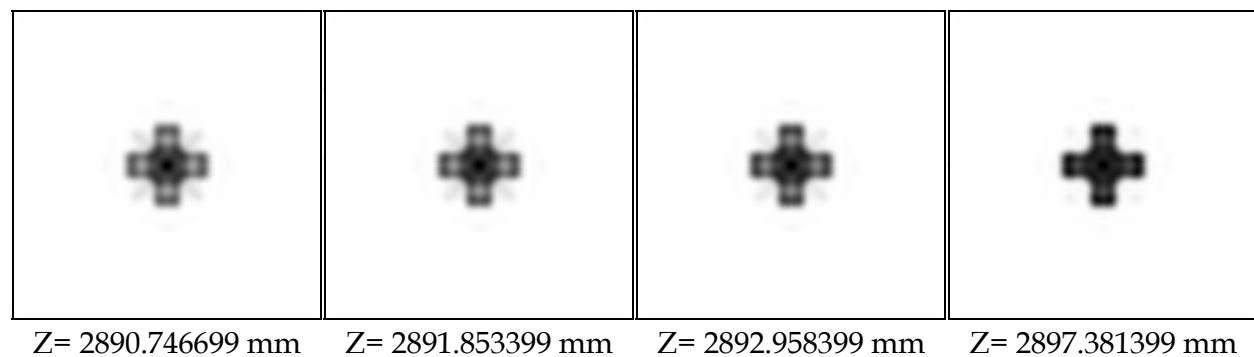
| Z= 2890.746699 mm | Z= 2891.853399 mm | Z= 2892.958399 mm | Z= 2897.381399 mm |

Fig. 15. Image self-reproduction – the "cross" image decomposition at different distances **z** from the second group of image self-reproduction points.

Figure 16 shows similar patterns of the decomposition of a triangle and a horizontal line-segment. Figure 17 shows examples of test superpositions composed of a few number of modes.

It should be noted that arbitrary mode superpositions propagated in a fiber appear to have the same local self-reproduction periods. This fact can be due to existence of general local periods for the entire set of modes propagated in the fiber. Because the self-reproduction periods for separate LG modes in a given fiber are similar and found in the range from 420 nm ((0,0) mode) to 426 nm (higher-order modes), the value of a local general period is much greater than an individual mode period.
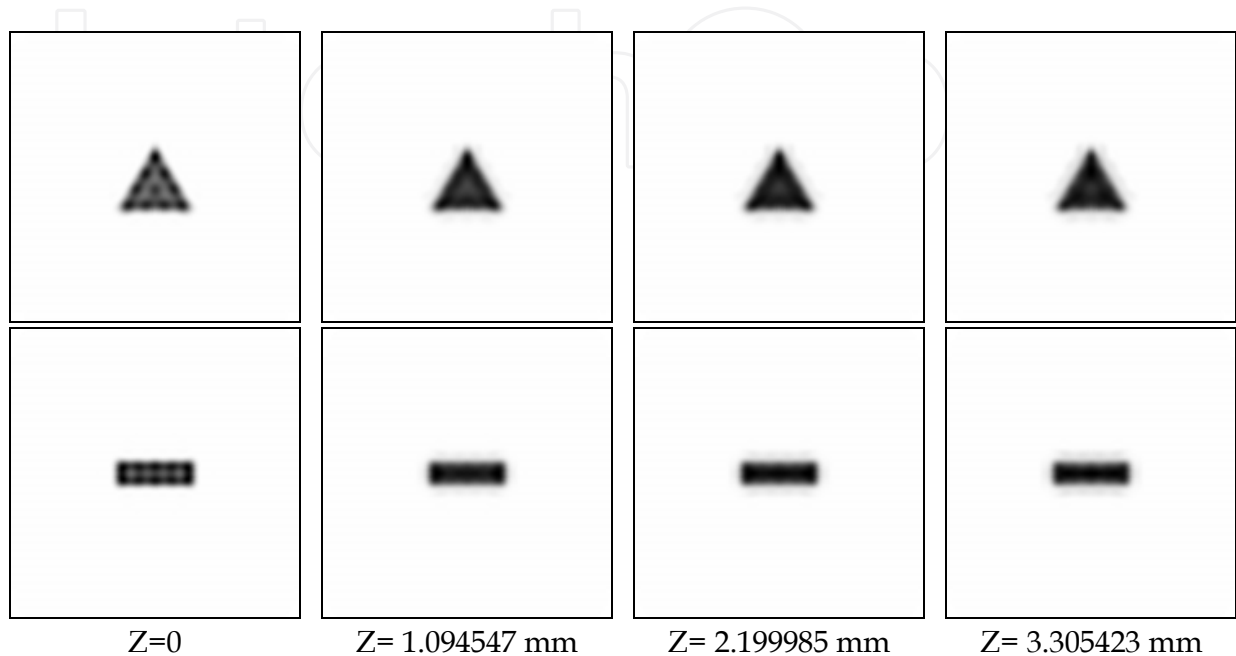

| Z=0 | Z= 1.094547 mm | Z= 2.199985 mm | Z= 3.305423 mm |

Fig. 16. Image self-reproduction – the "triangle" and "horizontal line" images decomposition at different distances **z** from the first group of image self-reproduction points.
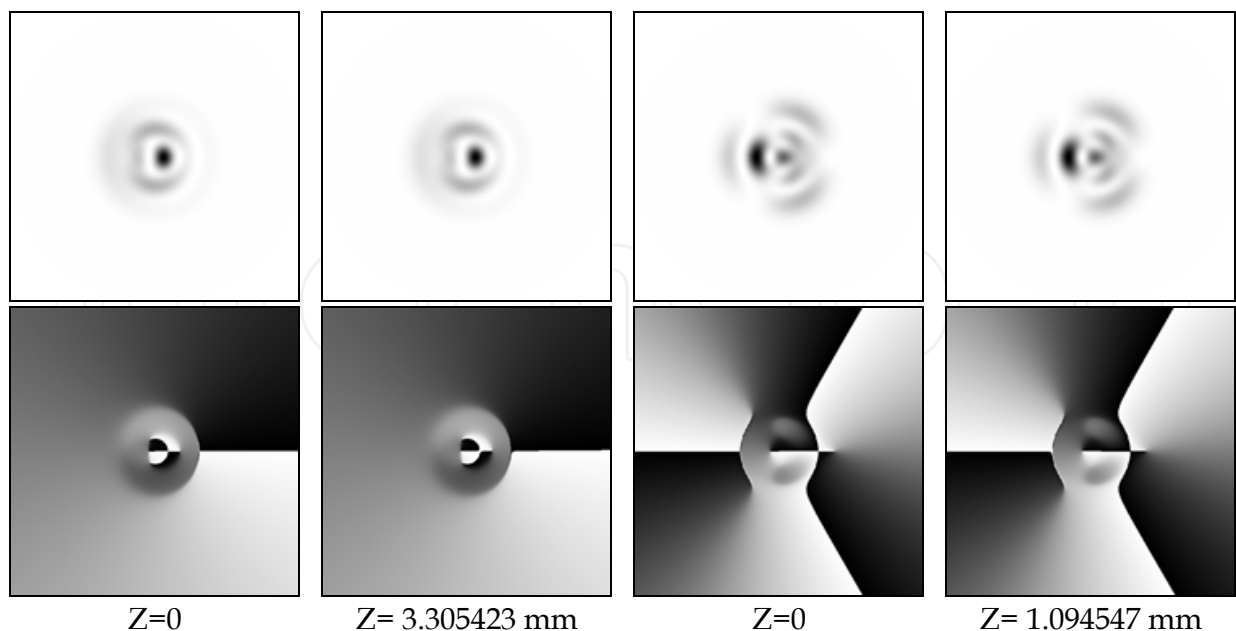

| Z=0 | Z= 3.305423 mm | Z=0 | Z= 1.094547 mm |

Fig. 17. Self-reproduction of the test mode decomposition (n,m): (0,-1)+(1,0)+(2,1) (the first and second columns), and (n,m): (0,1)+(1,3)+(2,0) (the third and fourth) at different distances **z** from the first group of image self-reproduction points.

It remains to note that finding the points of approximate image self-reproduction is a real computational challenge even for a comparatively small number of modes propagated in a 25 μm fiber. The problem is solved via successive search of the distance **Z** and finding a value at which all the quotients are integer. The method has other disadvantages. For example, it can provide only the boundaries of the intervals over which the desired mode composition is reproduced with a certain phase delay error, but is unable to identify an optimal within-interval point. This makes topical the development of a new, more efficient method of searching for the image self-reproduction points

3.2 Propagation of laser vortex beams in a parabolic optical fiber

The propagation of the electromagnetic wave in the medium can be modeled in several ways. The most common technique is to describe the propagation using Maxwell's equations, from which vectorial wave equations defining the electric and magnetic field components can be deduced. If the relative change of the medium refractive index per wavelength is significantly smaller than unity, the Helmholtz equation can be written for each scalar component of the vector field.

We have looked into the propagation of monochromatic light beams with helical phase singularity in a nonuniform medium, including a parabolic-index waveguide. We have proposed an approximation of the differential operator of propagation in a weakly nonuniform medium, which allows the propagation of light beams in the nonuniform medium to be treated as the propagation in a uniform medium through an array of thin optical elements. Using the limiting passage to an infinitely large number of lenses put at an infinitesimally small distance, a paraxial integral operator to describe the light field propagation in a parabolic medium has been derived (Khonina et al., 2010):

$$
E(x,y,z) \approx -\frac{ik\alpha}{2\pi\sin(\alpha z)}\exp\{ikz\}\exp\left\{\frac{ik\alpha}{2\tan(\alpha z)}\Big[x^2+y^2\Big]\right\}\times
$$
$$
\times \int\limits_{-\infty}^{\infty}\int\limits_{-\infty}^{\infty} E_0(\xi,\eta)\exp\left\{\frac{ik\alpha}{2\tan(\alpha z)}\Big[\xi^2+\eta^2\Big]\right\}\exp\left\{-\frac{ik\alpha}{\sin(\alpha z)}\Big[\xi x+\eta y\Big]\right\}d\xi d\eta.
$$

(30)

This integral operator makes it possible to simulate the propagation of arbitrarily shaped light beams, being indefinite in a general sense at distances multiple to the half-period. At $\alpha \to 0$ this integral operator is reduced to the Fresnel transform that describes, with the same accuracy, the propagation of light in a uniform medium. The integral in Eq. (30) has a period of $z_T = 2\pi/\alpha$.

At distances multiple to a quarter of period, the distribution $F(x,y,z) = E(x,y,z)\exp\{-ikz\}$ has the following specific features:

- at distance $z = z_T/4$, the distribution $F(x, y, z)$ is defined by the Fourier transform of the initial distribution;
- at distance $z = z_T/2$, the inverted distribution is formed: $-E_0(-x, -y)$;
- at distance $z = 3z_T/4$, the distribution $F(x, y, z)$ is the inverse Fourier transform of the initial distribution;
- at distance $z = z_T$, the initial distribution $E_0(x, y)$ is formed.

We performed the numerical simulation of the paraxial integral operator in Eq. (30) by the sequential integration method based on the quadrature Simpson formulae in a bounded

square region. In a general sense, the paraxial integral is not defined at distances multiple to $z_T / 2$, where the inverted and equi-initial intensity distributions are to be formed, so that the numerical simulation based on the quadrature formulae produces a completely erroneous result. At these distances, the integral in Eq. (30) needs to be treated in a general sense.

Figure 18 depicts the numerically simulated propagation of the LG mode $\Psi_{0,1}$ partially shielded with an opaque screen. The simulation is based on the paraxial integral operator in Eq. (30).

0	$z_T / 8$	$z_T / 4$	$3z_T / 8$	$7z_T / 8$
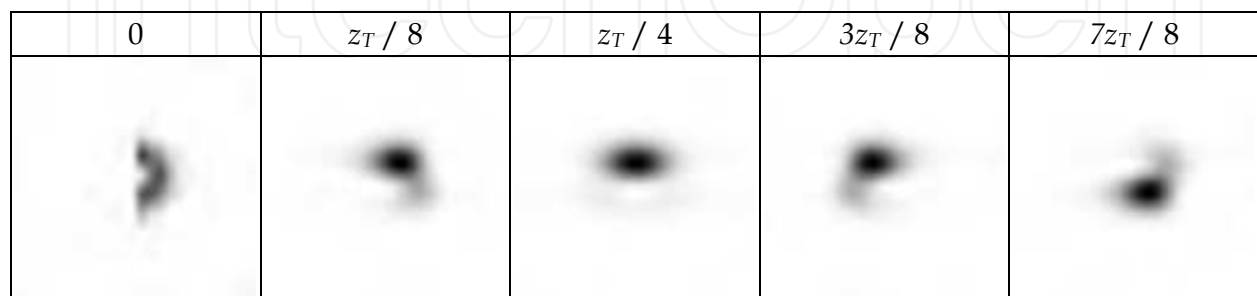
Fig. 18. Numerically simulated propagation of the mode $\Psi_{0,1}$ shielded by an aperture on the left ($\sigma = \sigma_0$).

The above results suggest that although the use of the integral operator makes it possible to model the propagation of arbitrarily shaped beams, computational challenges arise at definite distances on the optical axis.

An alternative method for modeling the propagation of light based on the decomposition of the input light beam into the medium eigenmodes has also been discussed. The effect of the operator in Eq. (30) on the LG modes can be found in (Striletz & Khonina, 2008). Here, we only give the final relation

$$\Psi_{nm}(r,\varphi,z) = \frac{1}{\sigma_0} \sqrt{\frac{n!}{\pi(n+|m|)!}} \frac{\sigma}{\sigma(z)} \left(\frac{r}{\sigma(z)}\right)^{|m|} L_n^{|m|}\left(\frac{r^2}{\sigma^2(z)}\right) \exp\left\{i\beta_{nm}(r,z) - \frac{r^2}{2\sigma^2(z)} + im\varphi\right\}, \quad (31)$$

where

$$\sigma(z) = \sigma\left[\cos^2(\alpha z) + \sigma_0^4 \sin^2(\alpha z)/\sigma^4\right]^{1/2} \quad (32)$$

is the effective radius of the LG mode;

$$\beta_{nm}(r,z) = kz + (2n+|m|+1)\left[\arctan\left\{\frac{\sigma^2}{\sigma_0^2} \frac{1}{\tan(\alpha z)}\right\} - \frac{\pi}{2}\right] + \left(1 - \frac{\sigma^2}{\sigma^2(z)}\right)\frac{1}{\tan(\alpha z)}\frac{r^2}{2\sigma_0^2} \quad (33)$$

is the function that defines the phase velocity.

In particular, when the waveguide is illuminated by the LG eigenmode ($\sigma = \sigma_0$), Eq. (31) takes the form of Eq. (25).

If the initial radius σ is smaller than the effective radius σ_0 of the fiber eigenmode, the beam radius $\sigma(z)$ at first increases, attaining a maximum of $\sigma_{max} = \sigma_0^2/\sigma$ at points

$z_s = \pi(s - 1/2)/\alpha$, $s \in \mathbf{N}$, where the Fourier image of the initial beam is formed. Then, the radius decreases, attaining a minimum of $\sigma_{\min} = \sigma_0$ at points $\sigma(z)$, $z_s = \pi s/\alpha$, $s \in \mathbf{N}$. However, if σ is larger than σ_0, then, $\sigma(z)$ at first decreases till $\sigma_{\min} = \sigma_0^2/\sigma$ and then increases up to the initial value.

Figure 19 shows the intensity distributions for a LG mode superposition, whose propagation is defined by Eq. (31).

The expansion coefficients for the Gaussian vortex beam have been deduced (Khonina et al., 2010) in the analytical form and can be used for the non-paraxial modeling.

0	$z_T / 8$	$z_T / 4$	$3z_T / 8$	$z_T / 2$
	$5z_T / 8$	$3z_T / 4$	$7z_T / 8$	z_T
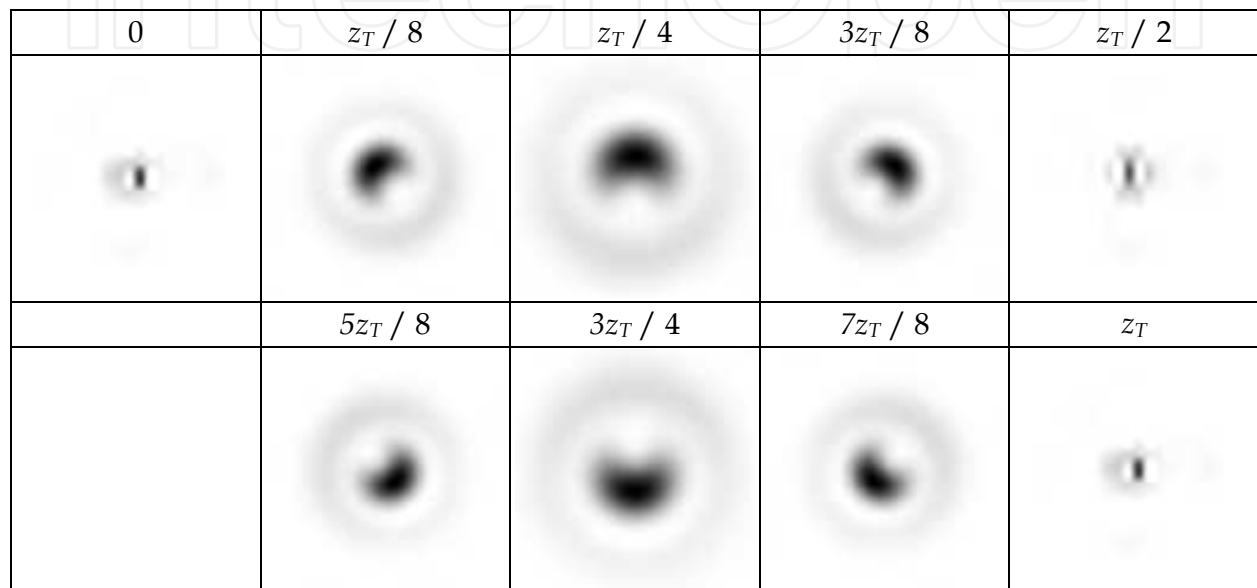
Fig. 19. Intensity distribution of the mode superposition $\Psi_{0,0} + \Psi_{1,-1}$ ($\sigma = \sigma_0/2$).

A Gaussian vortex beam with an arbitrary initial radius σ is given by

$$E_0(r,\varphi) = \frac{1}{\sigma\sqrt{\pi}} \exp\left\{-\frac{r^2}{2\sigma^2}\right\} \exp\{i\mu\varphi\},\tag{34}$$

where μ is an arbitrary constant.

The result of application of the integral operator in Eq. (30) to the input vortex beam in Eq. (34) is most easily represented by a superposition of the LG modes in Eq. (31) with z=0:

$$E_0(r,\varphi) = \sum_{n,m} C_{nm}\Psi_{nm}(r,\varphi,0)\tag{35}$$

Considering the normalization properties of the LG modes, the coefficients C_{nm} are defined as

$$C_{nm} = A_{n,m} \int_0^\infty \left(\frac{r}{\sigma}\right)^{|m|} L_n^{|m|}\left(\frac{r^2}{\sigma^2}\right) \exp\left\{-\frac{r^2}{\sigma^2}\right\} r\,dr \int_0^{2\pi} \exp\{i(\mu - m)\varphi\}\,d\varphi.\tag{36}$$

Using the replacement $\xi = r^2/\sigma^2$ and taking the integral with respect to the variable φ, we obtain

$$C_{nm} = \sqrt{\frac{n!}{(n+|m|)!}} \frac{\exp\{2\pi i(\mu-m)\}-1}{2\pi i(\mu-m)} \int_0^\infty \xi^{\frac{|m|}{2}} L_n^{|m|}(\xi)\exp\{-\xi\}\,d\xi. \tag{37}$$

Using the Laguerre polynomials in the form of Eq. (25) and integrating Eq. (37) n times by parts, we obtain

$$\int_0^\infty \xi^{\frac{|m|}{2}} L_n^{|m|}(\xi)\exp\{-\xi\}\,d\xi = \frac{1}{n!}\left(\frac{|m|}{2}\right)_n \int_0^\infty \xi^{\frac{|m|}{2}}\exp\{-\xi\}\,d\xi = \frac{1}{n!}\left(\frac{|m|}{2}\right)_n \Gamma\left(\frac{|m|}{2}+1\right), \tag{38}$$

where $(x)_n = \begin{cases} 1, & n=0 \\ x(x+1)\cdot...\cdot(x+n-1), n\neq 0 \end{cases}$; and $\Gamma(x)$ is Gamma function.

Finally, we obtain

$$C_{nm} = \frac{\left(\frac{|m|}{2}\right)_n \Gamma\left(\frac{|m|}{2}+1\right)}{\sqrt{(n+|m|)!n!}} \frac{\exp\{2\pi i(\mu-m)\}-1}{2\pi i(\mu-m)}. \tag{39}$$

If μ is integer, the expression in Eq. (39) is not equal to zero only at $m = \mu$. In this case, the propagation of the vortex beam in the parabolic fiber is described by a superposition of the functions in Eq. (31):

$$E(r,\varphi,z) = \sum_{n=0}^\infty \frac{\left(\frac{|\mu|}{2}\right)_n \Gamma\left(\frac{|\mu|}{2}+1\right)}{\sqrt{(n+|\mu|)!n!}} \Psi_{n,\mu}(r,\varphi,z). \tag{40}$$

Notice that the above relation also holds in a non-paraxial region because the modes in Eqs. (25) and (31) only differ by the propagation constant that has no effect on the decomposition coefficients.

Figure 20 respectively give the intensity, $|E(r,\varphi,z)|^2$, and phase, $\arg\{E(r,\varphi,z)\}$, distributions of the Gaussian beam in Eq. (34) for $\mu = 1$. The computations have been conducted using Eq. (40) for a finite number of terms ($n_{\max} = 50$) and by the numerical integration in Eq. (30). The figures suggest that there is a good qualitative agreement between the two methods. However, the numerical integration is seen to result in a minor asymmetry.

Propagation of vortex laser beam in a parabolic fiber has also been numerically simulated by the well known Beam Propagation Method (BPM) with use of BeamPROP simulation tool (RSoft Design, USA). The calculations were conducted for the wavelength of $\lambda = 633$ nm. The waveguide parameter $\alpha = 17.88$ mm⁻¹, $\alpha = 26.82$ mm⁻¹ and $\alpha = 35.76$ mm⁻¹, the waveguide width 30 μm, index on the waveguide axis $n_0 = 1.5$. Sampling step was 0.1 μm along x- and y- axes and 0.05 μm along z-axis. Simulation area has the sizes 90 μm along x- and y- axes and 300 μm along z-axis.

If the light field in initial plane $E_0(x, y)$ has the form of $A(r)\exp(in\varphi)$, it is obvious that intensity in transverse planes will be repeated with the period π/α instead of $2\pi/\alpha$. It can be seen in Fig. 21. For mentioned values of parameter α periods will be the following: $T = 175$ μm, $T = 120$ μm and $T = 88$ μm.

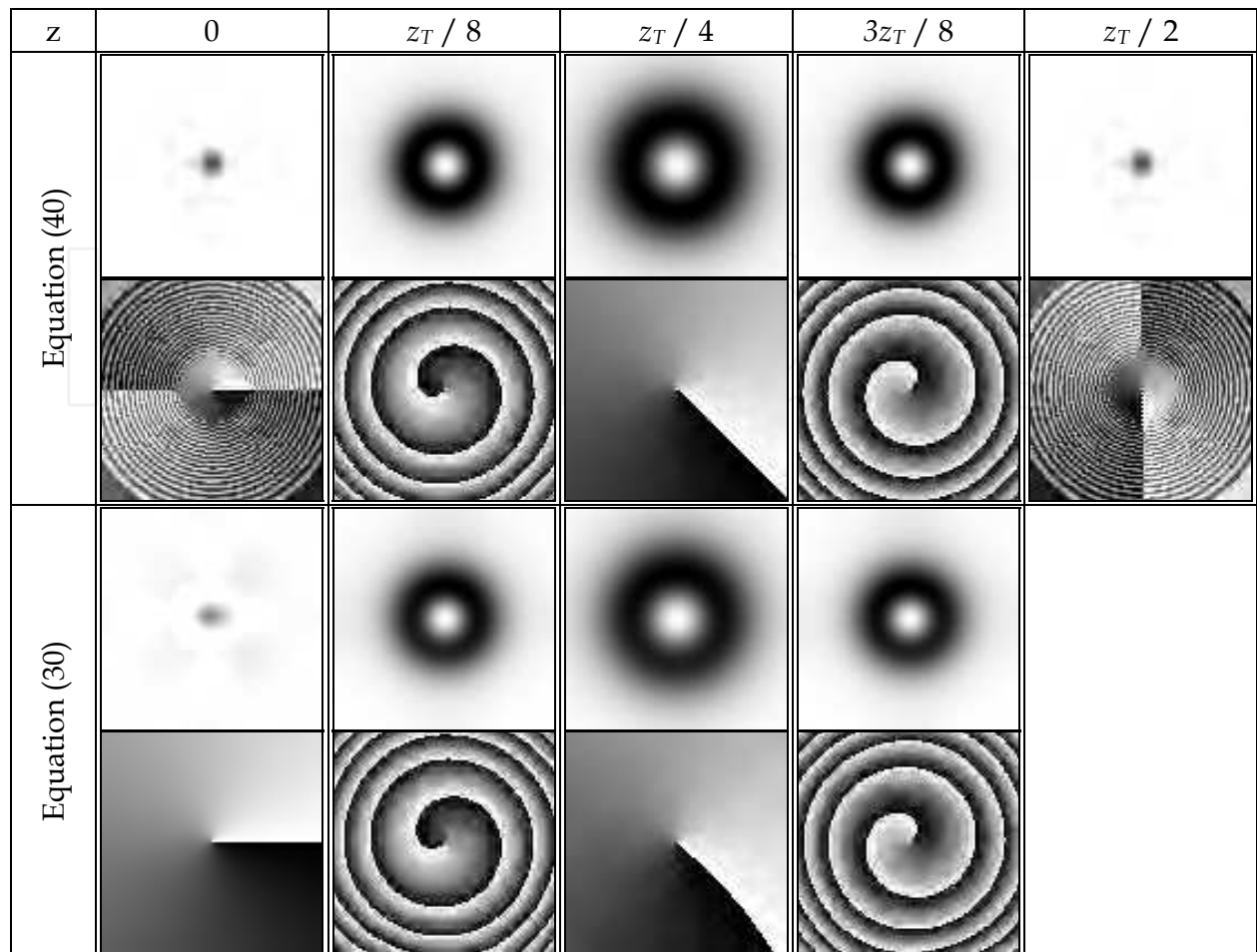| z	0	$z_T / 8$	$z_T / 4$	$3z_T / 8$	$z_T / 2$

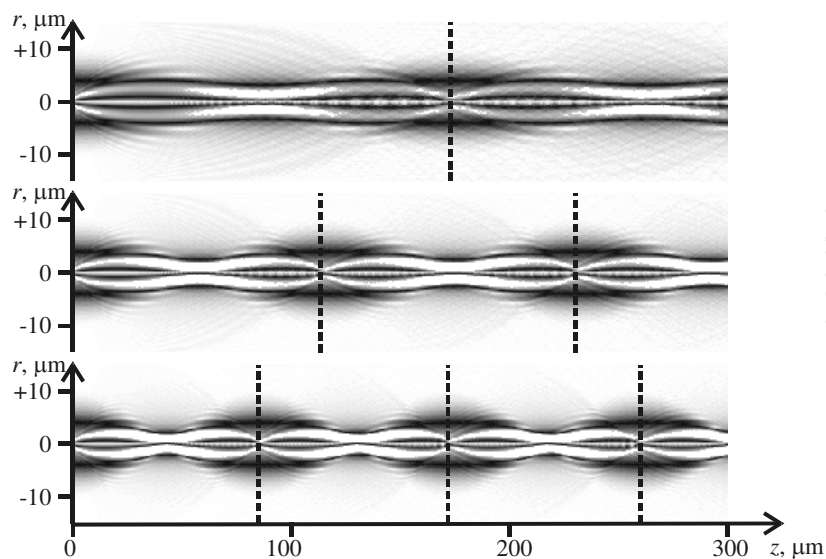Fig. 20. Propagation Gaussian optical vortex with $\mu = 1$ ($\sigma = \sigma_0/2$).

Fig. 21. Propagation of Gaussian optical vortex in parabolic waveguide for various values of parameter α: α = 17.88 mm⁻¹ (top part), α = 26.82 mm⁻¹ (central part) and α = 35.76 mm⁻¹ (bottom part). Dashed lines mean periods of diffraction patterns (i.e. planes $z = p\pi / \alpha$, where p are integer numbers).

| z = 0 | z = T/4 | z = T/2 | z = 3T/4 | z = T | z = 2T |
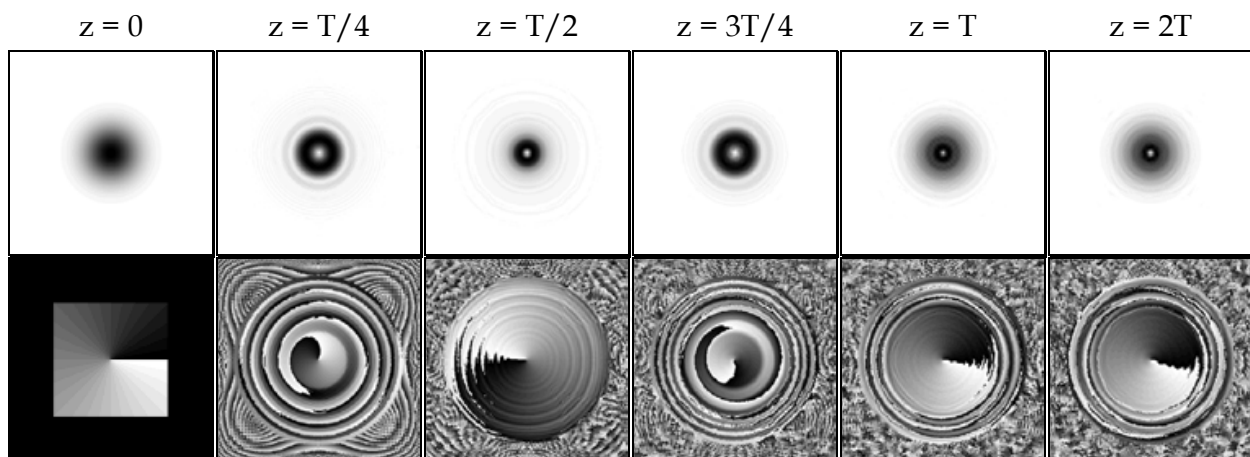
Fig. 22. Propagation Gaussian optical vortex with $\mu = 1$ using BPM.

So, variations in the transverse distribution of the light beam have been shown to be periodic for all beams other than fiber eigenmodes.

4. Conclusion

In this work:
- Linearly polarized modes of a weakly guiding fiber with a non-zero orbital angular momentum have been discussed. Conditions (expressed through the mode indices) for various self-reproduction types of multi-mode laser fields (invariance, rotation, periodic self-reproduction of the field transverse intensity distribution) have been deduced;
- An algorithm for generating a set of modal superpositions showing various self-reproduction properties to a designed accuracy has been developed;
- Experiments on excitation of lower-order angular harmonics and their superpositions in a stepped-index few-mode optical fiber have been conducted;
- An algorithm for finding the self-reproduction periods of a linear superposition of the Laguerre-Gauss modes in a circular graded-index fiber is developed. In terms of self-reproduction accuracy, various types of periods (local and general) have been identified. It has been found that arbitrary mode superpositions in a specific fiber have the same local self-reproduction periods, which is owing to the existence of general local periods of the entire set of the fiber modes.
- We have looked into the propagation of monochromatic light beams with helical phase singularity in a nonuniform medium, including a parabolic-index waveguide. Variations in the transverse distribution of the light beam have been shown to be periodic for all beams other than fiber eigenmodes.
- An alternative method for modeling the propagation of light based on the decomposition of the input light beam into the medium eigenmodes has also been discussed. The result of application of the integral operator to the non-paraxial Laguerre-Gauss modes with an arbitrary initial effective radius has been analytically derived.

The revealed features of vortex beams propagation in an optical fiber expand opportunities of fiber optics in various applications, including, additional compression of information channels and new degrees of freedom in coding and protection of the information.

5. References

Agrawal, G.P. (2002). *Fiber-Optic Communication Systems* (3rd Edition), John Wiley

Allen, L., Barnett, S.M., and Padget, M. J. (2003). *Optical Angular Momentum*, Institute of Physics, Bristol

Almazov, A.A., Khonina, S.N. (2004). Periodic self-reproduction of multi-mode laser beams in graded-index optical fibers. *Optical Memory and Neural Networks (Information Optics)*, Vol. 13, No. 1, pp. 63-70

Berdague, S., Facq, P. (1982). Mode division multiplexing in optical fibers. *Appl. Optics*, Vol. 21, pp. 1950-1955,

Bolshtyansky, M. A., Zel'dovich, B. Ya. (1996). Transmission of the image signal with the use of multimode fiber. *Optics Comm.*, Vol. 123, pp. 629-636

Bolshtyansky, M. A., Savchenko, A. Yu., Zel'dovich, B. Ya. (1999). Use of skew rays in multimode fibers to generate speckle field with nonzero vorticity. *Opt. Lett.*, Vol. 24, No. 7, pp. 433-435

Cherin, A.H. (1987). *An introduction to optical fibers*, McGraw-Hill book Co., Singapore

Dennis, M. R., O'Holleran, K., Padgett, M. J. (2009). Singular Optics: Optical Vortices and Polarization Singularities. *Progress in Optics*, Vol. 53, pp. 293-363

Desyatnikov, A. S., Kivshar, Yu. S., and Torner, L. (2005) Optical vortices and vortex solitons. *Progress in Optics*, ed. E. Wolf, Vol. 47, pp. 291-391, Elsevier, Amsterdam

Dubois, F., Emplit, Ph., and Hugon, O. (1994). Selective mode excitation in graded-index multimode fiber by a computer-generated optical mask. *Opt. Lett.*, Vol. 19, No. 7, pp. 433-435

Gloge, D. (1971). Weakly guided fibers. *Appl. Opt.*, Vol. 10, pp. 2252-2258

Karpeev, S. V., Pavelyev, V. S., Soifer, V. A., Khonina, S.N., Duparre, M., Luedge, B., Turunen, J. (2005). Transverse mode multiplexing by diffractive optical elements. *Proc. SPIE*, Vol. 5854, pp. 1-12

Karpeev, S.V., Khonina, S.N. (2007). Experimental excitation and detection of angular harmonics in a step-index optical fiber. *Optical Memory & Neural Networks (Information Optics)*, Vol. 16, No. 4, pp. 295-300

Khonina, S. N., Skidanov, R. V., Kotlyar, V. V., Jefimovs, K., Turunen, J. (2003). Phase diffractive filter to analyze an output step-index fiber beam. *Optical Memory & Neural Networks (Information Optics)*, Vol. 12, No. 4, pp. 317-324

Khonina, S. N., Striletz, A. S., Kovalev, A. A., Kotlyar, V. V. (2010). Propagation of laser vortex beams in a parabolic optical fiber. *Proceedings SPIE*, Vol. 7523, pp. 75230B-1-12

Kotlyar, V.V., Soifer, V.A., Khonina, S.N. (1998). Rotation of multimodal Gauss-Laguerre light beams in free space and in a fiber. *Optics and Lasers in Engineering*, Vol. 29, No. 4-5, pp. 343-350

Kotlyar, V. V., Khonina, S. N., Soifer, V. A., Wang, Y. (2002). Measuring the orbital angular momentum of the light field using a diffractive optical element. *Avtometriya*, Vol. 38, No. 3, pp. 33-44

Marcuse, D. (1972). *Light transmission optics*, Van Nostrand Reinhold Co., New York

Mikaelian, A.L. (1980). Self-focusing media with variable index of refraction. *Progress in Optics*, Vol. 27, pp. 279-345

Mikaelian, A. L. (1990). *Optical Methods in Informatics*, Moscow, Nauka (Science) Publishers

Snyder, A. W., Love, J. D. (1987). *Optical Waveguide Theory*, Moscow Radio & Sviaz Publishers

Soifer, V.A., Golub, M.A. (1994). *Laser beam mode selection by computer-generated holograms*, CRC Press, Boca Raton

Soskin, M. S., Vasnetsov, M. V. (2001). Singular optics. *Progress in Optics*, Vol. 42, pp. 219-76

Striletz, A. S., Khonina, S. N. (2008). Matching and analysis of methods based on use of the differential and integral operators to describe the laser light propagation in a weakly nonuniform medium. *Computer Optics*, Vol. 32, No. 1, pp. 33-38 – in Russian

Thornburg, W. Q., Corrado, B. J., and Zhu, X. D. (1994). Selective launching of higher-order modes into an optical fiber with an optical phase shifter. *Opt. Lett.,* Vol. 19, No. 7, pp. 454-456

Volyar, A. V., Fadeeva, T. A. (2002). Dynamics of topological multipoles: II. Creation, annihilation, and evolution of nonparaxial optical vortices. *Optics and Spectr.*, Vol. 92, No. 2, pp. 253-262

Yeh, C. (1990). *Handbook of fiber optics. Theory and applications*, Academic Press Inc., New York
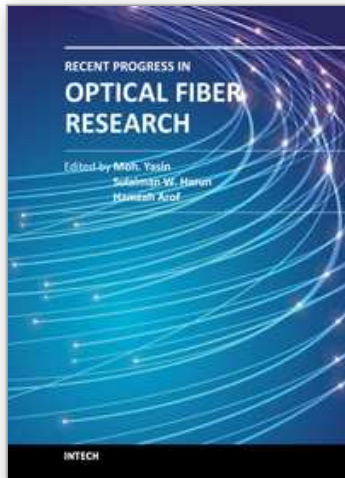
Recent Progress in Optical Fiber Research
Edited by Dr Moh. Yasin

This book presents a comprehensive account of the recent progress in optical fiber research. It consists of four sections with 20 chapters covering the topics of nonlinear and polarisation effects in optical fibers, photonic crystal fibers and new applications for optical fibers. Section 1 reviews nonlinear effects in optical fibers in terms of theoretical analysis, experiments and applications. Section 2 presents polarization mode dispersion, chromatic dispersion and polarization dependent losses in optical fibers, fiber birefringence effects and spun fibers. Section 3 and 4 cover the topics of photonic crystal fibers and a new trend of optical fiber applications. Edited by three scientists with wide knowledge and experience in the field of fiber optics and photonics, the book brings together leading academics and practitioners in a comprehensive and incisive treatment of the subject. This is an essential point of reference for researchers working and teaching in optical fiber technologies, and for industrial users who need to be aware of current developments in optical fiber research areas.

How to reference
In order to correctly reference this scholarly work, feel free to copy and paste the following:

S.N. Khonina, N.L. Kazanskiy and V.A. Soifer (2012). Optical Vortices in a Fiber: Mode Division Multiplexing and Multimode Self-Imaging, Recent Progress in Optical Fiber Research, Dr Moh. Yasin (Ed.), ISBN: 978-953-307-823-6, InTech, Available from: http://www.intechopen.com/books/recent-progress-in-optical-fiber-research/optical-vortices-in-a-fiber-mode-division-multiplexing-and-multimode-self-reproducing

INTECH
open science | open minds